A Comparative Study of Kalman Filtering for Sensorless Control of a Permanent-Magnet Synchronous Motor Drive

Borsje, P., Chan, T.F., Wong, Y.K. and Ho, S.L.
Department of EE, The Hong Kong Polytechnic University
Hong Kong, China

***Abstract*– This paper presents a comparative study of the novel Unscented Kalman Filter (UKF) and the Extended Kalman Filter (EKF) for estimation of the rotor speed and position of a permanent-magnet synchronous motor (PMSM) drive. The general structure of the EKF and the UKF are reviewed. The various system vectors, matrices, models and algorithm programs are presented. Simulation studies on the two Kalman filters are carried out using Matlab and Simulink to explore the usability of the UKF in a sensorless PMSM drive. In order to compare the estimation performances of the observers, both filters are designed for the same motor model and control system and run with the same covariances. The simulation results indicate that the UKF is capable of tracking the actual rotor speed and position provided that the elements of the covariance matrices are properly selected. Since covariance tuning of the Kalman filter is often a trial-and-error process, an unconventional, asymmetric way of setting the model covariance parameters is introduced. It is shown that tuning is easier and the method gives a significant improvement in performance and filter stability.**

I. INTRODUCTION

The permanent magnet synchronous motor (PMSM) is fast becoming the next-generation variable-speed AC motor drive due to the availability of high-energy permanent-magnet materials. Compared with the inverter-fed induction motor drive, the PMSM has no rotor loss and hence it is more efficient and a larger torque-to-weight ratio is achievable. One serious drawback of the classical PMSM, however, is the need for a rotor position sensor, such as a high-resolution encoder, for proper control of the inverter switches. To reduce the cost and to improve the reliability, sensorless PMSM control strategies have been developed. In these strategies, the motor position and speed is *estimated* and used as a feedback signal for closed-loop speed control.

The Kalman filter is a special kind of observer which provides optimal estimation of the system states based on least-square techniques. The extended Kalman filter (EKF) is widely used for nonlinear filter problems. It is derived from the Kalman filter based on the successive linearization of the signal process and observation map. The EKF has been successfully applied to several sensorless AC drives [1]-[11]. Although the EKF is straightforward and simple to apply, it has three important drawbacks:

1. Costly and sometimes complex derivation of the Jacobian/Hessian matrices.
2. Only first-order accuracy.
3. The linearization can lead to filter instability.

To overcome the above drawbacks, Julier and Uhlmann [12], [13] introduced a novel estimation tool, known as the Unscented Kalman filter (UKF) for replacing the EKF in nonlinear filtering problems. The main advantage of the UKF is that linearization of the state and covariances is no longer necessary. Instead of linearizing using Jacobian matrices, the UKF uses a deterministic sampling approach to capture the mean and covariance estimates with a minimal set of sample points. Although the UKF has been applied to a wide range of estimation problems [14]-[18], little research work has been done on its application to position and speed estimation in sensorless PMSM drives.

In this paper, we explore the potential benefits of the UKF over the widely used EKF for sensorless control of PMSM drives. We describe the results of simulation studies which examine the estimation performances of the UKF and EKF in a variety of drive operations for a PMSM drive. The simulation will be done with Matlab/Simulink software.

Like the EKF, the UKF also lacks analytical methods for suitable selection of model covariances. Choosing the parameters is often a trial-and-error process. Several methods have been introduced to find optimal settings [9]-[11]. In the present study, an unconventional way of choosing the model covariance parameters will be introduced.

This paper is organized as follows. The next section gives some design considerations for the chosen drive structure. In section III a description of the control structure for the sensorless drive can be found. In section IV the used PMSM motor model is presented. Section V gives a summary of the EKF and UKF filter. The simulation results are presented in section VI.

II. DESIGN CONSIDERATIONS

The motor model can be derived both in the stationary orthogonal $\alpha\beta$-reference frame, fixed to the stator, or in the synchronous dq-reference frame, fixed to the rotor flux.

When implemented using the $\alpha\beta$-reference frame, the Kalman filter may converge to the wrong solution ($-\omega$, $\theta+\pi$) [4]. The wrong solution is maintained by the innovation step which updates the estimate and compensate for the difference between actual and predicted voltages and currents. Simulation studies have proved that this, as expected, also

0-7803-8987-5/05/$20.00 ©2005 IEEE.

applies to the UKF. Dedicated algorithms need to be implemented to correct the wrong convergence at startup [1].

Using the PMSM model in the *dq*-reference frame, the wrong convergence solution will not fit in the voltage equations and, hence, will prevent the system from wrong startup. Another side effect is that the system state matrices are less complex, especially for the interior-type PMSM, which will reduce the computational requirements considerably [2]. The main disadvantage of the *dq* model for a PMSM is that the measured currents need to undergo a coordinate transformation which uses the *estimated* position. This will introduce errors in the measured currents which are used in the innovation step, resulting in a constant error in the position estimation.

In the model equations, the velocity ω is regarded as constant within the sampling time step T_s, assuming that the electrical system's time constant is much smaller than the mechanical time constant. The motor inductances are assumed to be independent of currents, i.e., saturation effects arenot taken into account.

III. Speed and Current Controller

Fig. 1 shows a schematic diagram of the proposed sensorless PMSM drive. A proportional-plus-integral (PI) speed controller is implemented to regulate the rotor speed by comparing the reference speed with the estimated speed. The PI controller delivers an output current reference i_q*, while the direct current reference i_d* is set to zero for normal operation in order to obtain the maximum torque-to-current ratio.

Fig. 2 shows the schematic diagram of the current controller represented using Simulink blocks. Two PI controllers are employed to regulate the stator current and feedforward control is used to decouple the dynamics between the applied voltages and the currents. The inputs of the current controller are the current reference and the estimated rotor speed, while its output is the reference voltage. The reference voltage will be applied to a space vector pulse width modulation (SVPWM) unit. The outputs of the PI controllers are limited and have anti-reset windup.

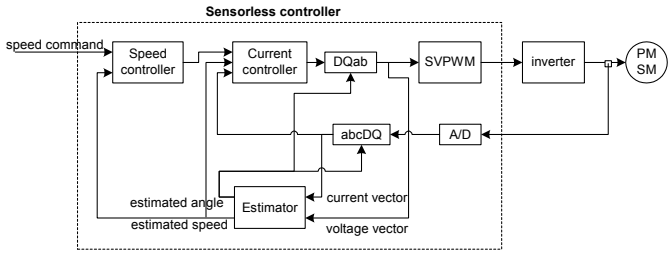

Fig. 1 Schematic diagram of proposed sensorless PMSM drive.

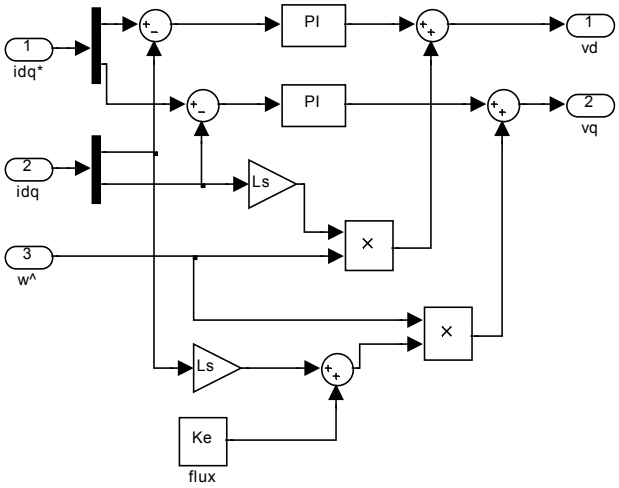

Fig. 2 Current controller: a representation using Simulink blocks.

The reference voltages are used as estimator input instead of the measured phase voltages in order to improve the drive's robustness to noise without the need for filtering. This approximation, however, is not effective at low speeds because of the dead times and the voltage drop of the inverter bridge, causing relatively large errors in the voltage estimate. Compensation methods can be used to improve the performance at low speeds [2], [20]-[22].

IV. PMSM Equations

To avoid convergence problems at startup and to simplify the motor equations, the rotor reference frame is chosen for evaluation of the Kalman filters [2]. The motor nonlinear state equations can be expressed in the form:

$$\begin{aligned}\dot{\mathbf{x}}(t) &= \mathbf{F}\left(\mathbf{x}(t)\right)\mathbf{x}(t) + \mathbf{G}\mathbf{u}(t)\\ \mathbf{y}(t) &= \mathbf{H}\mathbf{x}(t)\end{aligned} \tag{1}$$

where $\mathbf{u} = \begin{bmatrix} u_d & u_q \end{bmatrix}'$ and $\mathbf{y} = \begin{bmatrix} i_d & i_q \end{bmatrix}'$ are the input and the output vectors, respectively. The state variables are $\mathbf{x} = \begin{bmatrix} i_d & i_q & \omega_e & \theta_e \end{bmatrix}'$

The system state matrices are defined as

$$\mathbf{F}\left(x(t)\right) = \begin{bmatrix} -\dfrac{R}{L_d} & \omega_e \dfrac{L_q}{L_d} & 0 & 0 \\ -\omega_e \dfrac{L_d}{L_q} & -\dfrac{R}{L_q} & -\dfrac{K_e}{L_q} & 0 \\ 0 & 0 & 0 & 0 \\ 0 & 0 & 1 & 0 \end{bmatrix} \tag{2}$$

$$\mathbf{G} = \begin{bmatrix} \frac{1}{L_d} & 0 \\ 0 & \frac{1}{L_q} \\ 0 & 0 \\ 0 & 0 \end{bmatrix} \quad \mathbf{H} = \begin{bmatrix} 1 & 0 \\ 0 & 1 \\ 0 & 0 \\ 0 & 0 \end{bmatrix} \tag{3)(4}$$

As can be seen from Fig. 1, the measurement of the phase voltages is replaced by the actual *dq* voltage delivered by the current control.

V. Estimation Strategies

A. EKF algorithm

The EKF is an optimal estimator in the least square sense for the estimation of nonlinear dynamic systems. It is derived from the Kalman filter based on successive linearization of the signal process and observation map [14]. More details can be found in a previous work [3].

For this application the motor nonlinear state equations (1) are expressed in the discretized form

$$\mathbf{x}_{k+1} = \mathbf{F}_\mathbf{d}\left(\mathbf{x}_k\right)\mathbf{x}_k + \mathbf{G}_\mathbf{d}\mathbf{u}_k + \mathbf{w}_k \tag{5}$$

$$\mathbf{y}_k = \mathbf{H}_\mathbf{d}\mathbf{x}_k + \mathbf{v}_k \tag{6}$$

The state model represented by (5) and (6) also includes the statistical description for the inaccuracies, where $\mathbf{w}_k = \mathbf{w}\left(kT_s\right)$ and $\mathbf{v}_k = \mathbf{v}\left(kT_s\right)$ are, respectively, the zero-mean Gaussian process noise and measurement noise vectors with covariance matrices **Q** and **R**.

The discretized matrices are derived using the exponential Taylor approximation [23]-[24], assuming a small sampling time and the use of zero-order-hold (ZOH) sampling technique.

$$\mathbf{F}_\mathbf{d} \cong \mathbf{I} + \mathbf{F}T_s \tag{7}$$

$$\mathbf{G}_\mathbf{d} \cong \mathbf{G}T_s \tag{8}$$

$$\mathbf{H}_\mathbf{d} = \mathbf{H} \tag{9}$$

The basic idea of the EKF is to linearize the state-space model represented by (5) and (6) at each time instant around the most recent state estimate, which is taken at $\hat{\mathbf{x}}_k$ or $\hat{\mathbf{x}}_{k-1}$. Once a linear model is obtained, the standard Kalman filter equations can be applied.

The prediction of the state covariance requires the online computation of Jacobian matrix **Φ,** defined as

$$\mathbf{\Phi}_{k-1} = \left.\frac{\partial \mathbf{F}\left(\mathbf{x}(t)\right)\mathbf{x}(t)}{\partial \mathbf{x}}\right|_{\mathbf{x}=\hat{\mathbf{x}}_{k|k-1}} = \left.\frac{\partial \dot{\mathbf{x}}}{\partial \mathbf{x}}\right|_{\mathbf{x}=\hat{\mathbf{x}}_{k|k-1}} \tag{10}$$

The Jacobian of **H** is not calculated because **H** is linear. The discretized Jacobian of $\mathbf{\Phi}_{k-1}$ will be approximated with

$$\mathbf{\Phi}_{\mathbf{d},k-1} \cong \mathbf{I} + \mathbf{\Phi}_{k-1}T_s \tag{11}$$

For a given sampling time t_k the optimal state estimation $\hat{\mathbf{x}}_{k|k}$ and its covariance matrix $\hat{\mathbf{P}}_{k|k}$ are generated by the filter through a two-step loop. The first step performs a prediction of both quantities using the previous estimates $\hat{\mathbf{x}}_{k|k-1}$ and the mean voltage vector $\left\langle \mathbf{u}_{k-1} \right\rangle$ actually applied to the system in the period t_{k-1} to t_k. The second step corrects the predicted state estimate and covariance matrix by the measured actual motor phase currents.

Step 1: Prediction (time update)

$$\hat{\mathbf{x}}_{k|k-1} = \mathbf{F}_\mathbf{d}\left(\hat{\mathbf{x}}_{k-1|k-1}\right)\hat{\mathbf{x}}_{k-1|k-1} + \mathbf{G}_\mathbf{d}\left\langle \mathbf{u}_{k-1} \right\rangle \tag{12}$$

$$\mathbf{P}_{k|k} = \mathbf{\Phi}_{\mathbf{d}k-1}\mathbf{P}_{k-1|k-1}\mathbf{\Phi}_\mathbf{d}{}'_{k-1} + \mathbf{Q}_\mathbf{d} \tag{13}$$

Step 2: Innovation (measurement update)

$$\hat{\mathbf{x}}_{k|k} = \hat{\mathbf{x}}_{k|k-1} + \mathbf{K}_k\left(\mathbf{y}_k - \mathbf{H}\hat{\mathbf{x}}_{k|k-1}\right) \tag{14}$$

$$\mathbf{P}_{k|k} = \mathbf{P}_{k|k-1} - \mathbf{K}_k\mathbf{H}\mathbf{P}_{k|k-1} \tag{15}$$

The Kalman gain is calculated by

$$\mathbf{K}_k = \mathbf{P}_{k|k-1}\mathbf{H}'\left[\mathbf{H}\mathbf{P}_{k|k-1}\mathbf{H}' + \mathbf{R}_\mathbf{d}\right]^{-1} \tag{16}$$

The covariance update involves subtraction and can result in loss of symmetry and positive definiteness due to rounding errors. Joseph's form covariance update [14] avoids this at the expense of some computational burden:

$$\mathbf{P}_{k|k} = \left[\mathbf{I} - \mathbf{K}_k\mathbf{H}_{k-1}\right]\mathbf{P}_{k|k-1}\left[\mathbf{I} - \mathbf{K}_k\mathbf{H}_{k-1}\right]^{-1} + \mathbf{K}_k\mathbf{R}_\mathbf{d}\mathbf{K}'_k \tag{17}$$

Details of the Jacobian matrices are given in Appendix A.

B. Unscented Kalman filter

The UKF is a derivative free alternative to the EKF [14]. The basic mechanism for UKF is the same as the one described above by the equations (12) and (14). The difference is that the UKF performs the state estimation *by approximating the probability distribution <u>after</u> performing the computation using the nonlinear function,* rather than approximating the nonlinearity itself as in the EKF. To do this, the UKF utilizes the so called *Unscented Transformation* (UT).

A set of deterministic sample points is taken around the last known state and propagated through the real nonlinear function. With these results a mean and covariance can be approximated using a weighted sample mean and covariance of the transferred sample points.

These weighted sample points are generated as follows. Consider the state variable **x** with dimension *L* having mean $\hat{\mathbf{x}}$ and covariance $\mathbf{P}_\mathbf{x}$. We now choose a set of $2L+1$ weighted samples χ_i (sigma points) deterministically so that they completely represent the true mean and covariance of state **x**.

$$\chi_0 = \hat{\mathbf{x}}$$
$$\chi_i = \hat{\mathbf{x}} + \left(\sqrt{(L+\lambda)\mathbf{P}_{\mathbf{x}}}\right)_i \qquad i = 1,...,L \tag{18}$$
$$\chi_i = \hat{\mathbf{x}} - \left(\sqrt{(L+\lambda)\mathbf{P}_{\mathbf{x}}}\right)_i \qquad i = n+1,...,L$$

$$W_0^{(m)} = \lambda/(L+\lambda)$$
$$W_0^{(c)} = W_0^{(m)} + 1 - \alpha^2 + \beta \tag{19}$$
$$W_i^{(m)} = \frac{1}{2(L+\lambda)} \qquad i = 1,...,2L$$

where $\lambda = \alpha^2(L+\kappa) - L$ is a scaling parameter. The superscripts $^{(m)}$ and $^{(c)}$ indicate the weight point for mean or covariance calculation respectively. The constant α determines the spread of the sigma points around $\bar{\mathbf{x}}$, and is set to a small positive value (e.g., $1 \le \alpha \le 10^{-4}$). The constant κ is a secondary scaling parameter which is usually set to (3–L), and β is used to include prior knowledge of the distribution of $\bar{\mathbf{x}}$ (for Gaussian distribution $\beta = 2$ is optimal).

$\left(\sqrt{(L+\lambda)\mathbf{P}_{\mathbf{x}}}\right)_i$ is the i-th row or column of the matrix square root of $(L+\lambda)\mathbf{P}_{\mathbf{x}}$, and W_i is the weight associated with the i-th sigma point so that $\sum_{i=0}^{2L} W_i = 1$. Now each point is propagated through the nonlinear function to yield a set of transformed sigma points,

$$Y_i = \mathbf{g}(\chi_i) \qquad i = 0,...2L \tag{20}$$

The mean and covariance of $\mathbf{y}$ are approximated by the weighted average mean and covariance of the transformed sigma points.

$$\hat{\mathbf{y}} = \sum_{i=0}^{2L} W_i Y_i$$
$$\mathbf{P}_{\mathbf{y}} = \sum_{i=0}^{2L} W_i (Y_i - \hat{\mathbf{y}})(Y_i - \hat{\mathbf{y}})^T \tag{21}$$

The UKF is an extension of the UT to the Kalman filter framework. Table I shows the standard UKF algorithm for the additive (zero mean) case which is used for the simulations.

VI. Simulation Results

To verify the state estimation performance of the UKF and the EKF, a number of simulations were carried out for different operating conditions and parameter settings. The simulations were implemented using Matlab/Simulink software. The EKF and UKF algorithms were implemented as s-function blocks which were then inserted into the Simulink model. The parameters of the motor model and simulation are given in Appendix B. A sampling time of 50μs was chosen for the s-function.

TABLE I
UKF Algorithm for Additive (Zero Mean) Noise

Initialize the state mean and covariance

for k=1, ...,∞

1. Calculate the sigma points χ_{k-1} using equations (18)(19)

2. Predict (time update):

$$\chi_{k|k-1} = \mathbf{F}\left[\chi_{k|k-1}, u_{k|k-1}\right]$$
$$\hat{\mathbf{x}}_k^- = \sum_{i=0}^{2L} W_i^{(m)} \chi_{i,k|k-1}$$
$$\mathbf{P}_k^- = \sum_{i=0}^{2L} W_i^{(c)} \left[\chi_{i,k|k-1} - \hat{\mathbf{x}}_k^-\right]\left[\chi_{i,k|k-1} - \hat{\mathbf{x}}_k^-\right]^T + \mathbf{Q}$$

3. Correct (measurement update):

$$Y_{k|k-1} = \mathbf{H}\left[\chi_{k|k-1}\right]$$
$$\hat{\mathbf{y}}_k^- = \sum_{i=0}^{2L} W_i^{(m)} Y_{i,k|k-1}$$
$$\mathbf{P}_{\mathbf{y}_k\mathbf{y}_k} = \sum_{i=0}^{2L} W_i^{(c)} \left[Y_{i,k|k-1} - \hat{\mathbf{y}}_k^-\right]\left[Y_{i,k|k-1} - \hat{\mathbf{y}}_k^-\right]^T + \mathbf{R}$$
$$\mathbf{P}_{\mathbf{x}_k\mathbf{y}_k} = \sum_{i=0}^{2L} W_i^{(c)} \left[\chi_{i,k|k-1} - \hat{\mathbf{x}}_k^-\right]\left[Y_{i,k|k-1} - \hat{\mathbf{y}}_k^-\right]^T$$
$$\mathbf{K}_k = \mathbf{P}_{\mathbf{x}_k\mathbf{y}_k}\mathbf{P}_{\mathbf{y}_k\mathbf{y}_k}^{-1}$$
$$\hat{\mathbf{x}}_k = \hat{\mathbf{x}}_k^- + \mathbf{K}_k\left(\hat{\mathbf{y}}_k - \hat{\mathbf{y}}_k^-\right)$$
$$\mathbf{P}_k^- = \mathbf{P}_k^- - \mathbf{K}_k\mathbf{P}_{\mathbf{y}_k\mathbf{y}_k}\mathbf{K}_k^T$$

where $\mathbf{Q}$ and $\mathbf{R}$ are the process and measurement covariances.

A crucial step in the design of the Kalman filters is the choice of the elements of the covariance matrices $\mathbf{Q}$ and $\mathbf{R}$, as they will affect the performance, convergence and stability. The use of large values in $\mathbf{Q}$ presumes high model noise and/or parameter uncertainties. An increase in the values of the elements of $\mathbf{Q}$ will likewise increase the Kalman gain, resulting in faster filter dynamics but poorer steady-state performance. Matrix $\mathbf{R}$ is related to the measurement noise. Increasing the values of the elements of $\mathbf{R}$ will assume that the current measurements are more affected by noise and thus less reliable. Consequently, the filter gain will decrease, yielding poorer transient response.

The covariances $\mathbf{Q}$ and $\mathbf{R}$ are fixed for the simulations. Different values have been experimented for $\mathbf{Q}$ and $\mathbf{R}$. For the simulation and comparison the following values were chosen:

$$\mathbf{P}_0 = \begin{bmatrix} 1 & 0 & 0 & 0 \\ 0 & 1 & 0 & 0 \\ 0 & 0 & 1 & 0 \\ 0 & 0 & 0 & 1 \end{bmatrix} \tag{22}$$

$$\mathbf{Q} = \begin{bmatrix} 0.4 & 0 & 0 & 0 \\ 0 & .004 & & 0 \\ 0 & 0 & 200 & 0 \\ 0 & 0 & 0 & 2 \end{bmatrix} \tag{23}$$

$$\mathbf{R} = \begin{bmatrix} .5 & 0 \\ 0 & .5 \end{bmatrix} \tag{24}$$

In (23), Q_{11} and Q_{22} were not set to be equal as is normally done. Various simulation experiments conducted have shown that this gives a good transient response as well as good steady-state performance. Also finding a stable set proved to be easier when Q_{22} is 10 to 100 times smaller than Q_{11}. The parameters for the UKF were set as follows: $\alpha = 1,\ \beta = 2,\ \kappa = 0$.

Fig. 3 and Fig. 4 show, respectively, the simulation results of UKF and EKF state estimation performance for the sensorless PMSM drive. It is observed that both the UKF and EKF are capable of tracking the motor states satisfactorily.

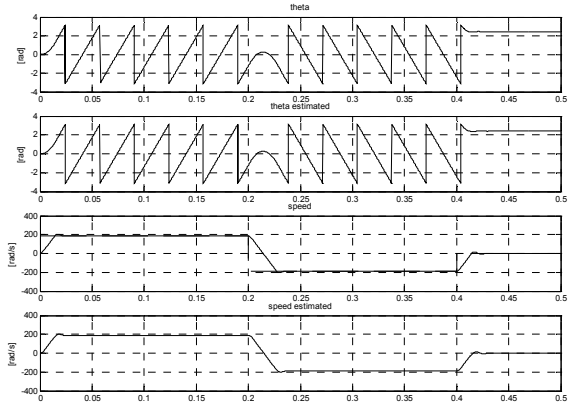

Fig. 3 UKF performance: motor angle and speed states for no-load four quadrant high-speed reversal.

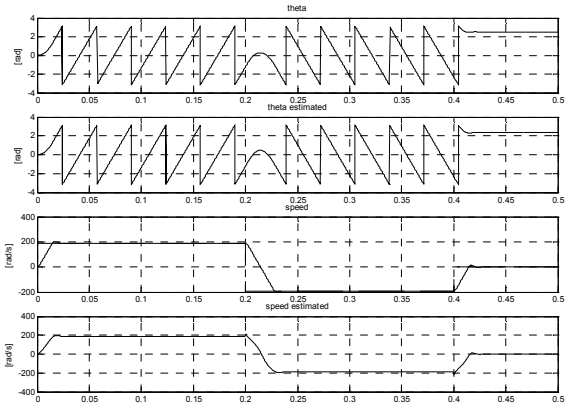

Fig. 4 EKF performance: motor angle and speed states for no-load four quadrant high-speed reversal.

To test the noise robustness of the Kalman filters, a current noise in the range of [0-0.5A] was injected into the measured currents. The same simulations were carried out as for Fig. 3 and Fig. 4. Fig. 5 and Fig. 6 show the errors between the actual and estimated states of the PMSM during this noise performance investigation. It can be observed that both filters were capable of tracking the speed and angle under noisy machine operation and the filter performances were comparable to the cases when no noise was present.

Fig. 7 and Fig. 8 show the speed estimation performance of the filters subsequent to step load changes. The PMSM is started on no load and accelerated to the command speed. At time t = 0.2 s, rated torque is applied to the motor. At t = 0.4 s, the load is removed. The simulation results show that both filters give similar performances under steady-state conditions, but with the UKF the motor speed exhibits more oscillations during the transient period before settling to the steady state. For the studied PMSM, the transient periods for UKF and EKF are 0.05 s and 0.03 s, respectively.

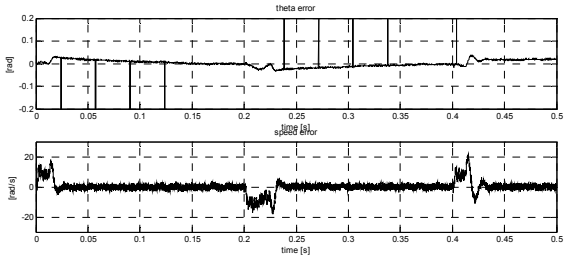

Fig. 5 UKF performance: angle error $(\theta_e - \hat{\theta}_e)$ and speed error $(\omega_m - \hat{\omega}_m)$ for no-load four-quadrant high-speed reversal with injected current noise.

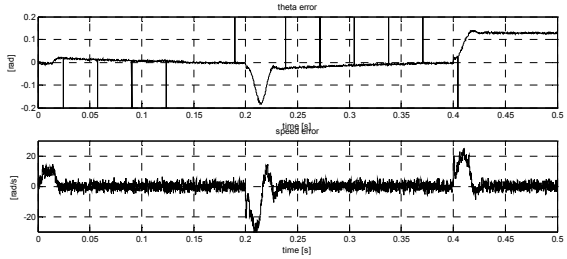

Fig. 6 EKF performance: angle error $(\theta_e - \hat{\theta}_e)$ and speed error $(\omega_m - \hat{\omega}_m)$ for no-load four-quadrant high-speed reversal with injected current noise.

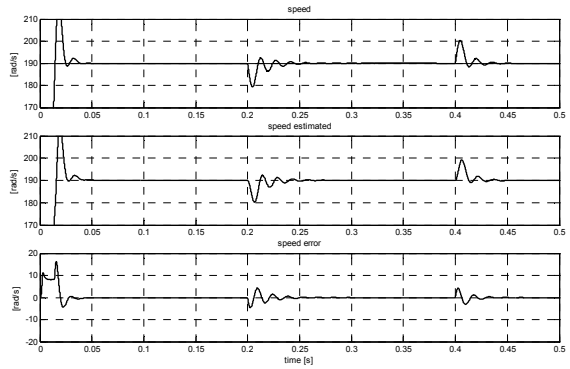

Fig. 7 UKF performance: speed response to step load changes at normal speed.

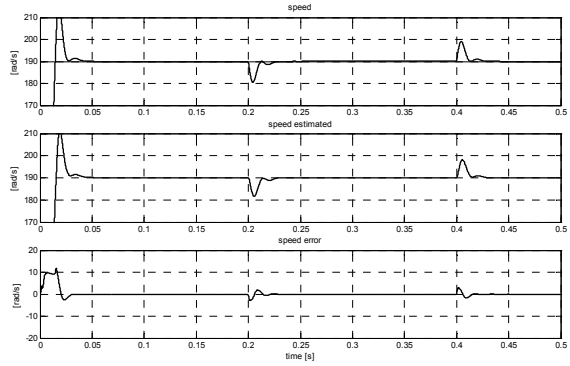

Fig. 8 EKF performance: speed response to step load changes at normal speed.

VII. COMPARISON

To compare the speed estimation of the EKF and UKF in more detail, the estimation errors are squared and accumulated during the simulation run. The results are shown in Fig. 9 for the no-load, full speed four-quadrant simulation cases shown in Fig. 3 and Fig. 4.

It can be seen that during startup the EKF performs slightly better than UKF. During the speed reversal, however, the UKF performs better, resulting in a much lower accumulated error count. Both estimators give good steady-state performance. After a transient period, the estimation error tends to zero, as observed from the horizontal lines in Fig. 9.

The transient response of the EKF seems slightly better; the steady-state (horizontal line) condition is reached in a shorter time.

The noise performance of the UKF seems better. Comparing Fig. 5 with Fig. 6, it can be observed that the speed estimate of the UKF is less noisy than that of the EKF as indicated by the thinner speed error trace.

The steady-state performance of both filters is similar. The dynamic response of the EKF, however, is better as can be seen from Fig. 7 and Fig. 8.

For a real-time implementation of the filters, the computation time of the control algorithms is another important factor. The EKF is designed for nonlinear systems; it linearizes the system at each sampling time by taking the derivative of the system matrices. This requires a costly 4x4 Jacobian matrix calculation for the PMSM model for every sampling time. Depending on the model used, this linearization can also introduce errors which may lead to system instability.

The UKF has a derivative-free structure and involves no linearization steps, which eliminates the need for the costly Jacobian calculation. The UKF however needs to calculate the sigma points for every sampling period. Depending on the system nonlinearities and complexity, the UKF can be a better alternative to EKF from computational requirement considerations.

A review of the s-function codes for the EKF and UKF shows that the computational requirements are less for EKF in the present application due to the relatively simple motor model and weak nonlinearity.

In other cases (for example, the IPM in [2]), the UKF can be used in the $\alpha\beta$-reference frame. This was not even possible for the EKF due to the complex Jacobian matrix calculations involved.

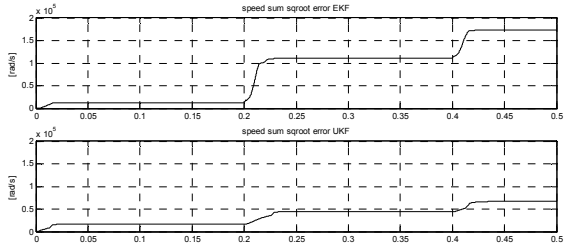

Fig. 9 Accumulated speed error at no load, full speed four quadrant simulation run.

VIII. CONCLUSIONS

Two different Kalman filtering techniques have been studied and compared. Both observers are found to be suitable candidates for sensorless control of PMSM drives. The EKF performs slightly better during motor start-up, but the UKF performs better in tracking the speed, especially during transients. For industrial applications where steady-state performance is critical, there is no preference for either filter. Under noisy conditions the UKF seems more promising with better filter characteristics than the EKF. In highly nonlinear and complex systems, the UKF is a serious competitor of the EKF. The computational requirements become in favor of the UKF due to the absence of the Jacobian matrix, making it possible to choose more complex and more accurate motor models that provide better performance. For simple motor drive models, however, the EKF is still the better choice as the algorithms and models are easier to optimize for real-time implementation, resulting in higher performance and lower costs for the microprocessor unit.

ACKNOWLEDGMENTS

The work described in this paper was fully supported by a grant from the Research Grants Council of the Hong Kong Special Administrative Region, China (Project No. PolyU 5201/03E).

APPENDIX A
CALCULATION OF JACOBIAN MATRICES F AND H

At time $t_{k-1} = (k-1)T_s$ the Jacobian matrix **F** is defined as in (2)

$$\mathbf{\Phi}_{k-1} = \left.\frac{\partial \mathbf{F}(\mathbf{x}(t))\mathbf{x}(t)}{\partial \mathbf{x}}\right|_{\mathbf{x}=\hat{\mathbf{x}}_{k|k-1}} = \left.\frac{\partial \dot{\mathbf{x}}}{\partial \mathbf{x}}\right|_{\mathbf{x}=\hat{\mathbf{x}}_{k|k-1}} \tag{23}$$

$$\dot{\mathbf{x}} = \begin{bmatrix} -\frac{R}{L_d} i_d + \omega_e \frac{L_q}{L_d} i_q + \frac{u_d}{L_d} \\ -\omega_e \frac{L_d}{L_q} i_d - \frac{R}{L_q} i_q - \frac{\lambda}{L_q} \omega_e \\ 0 \\ \omega_e \end{bmatrix} \tag{24}$$

F is a 4x4 matrix as follows:

$$\mathbf{F} = \begin{bmatrix} F_{11} & F_{12} & F_{13} & 0 \\ F_{21} & F_{22} & F_{23} & 0 \\ 0 & 0 & 0 & 0 \\ 0 & 0 & F_{43} & 0 \end{bmatrix} \tag{25}$$

The elements of matrix **F** at time $t_{k-1} = (k-1)T_s$ can be derived as follows:

$$F_{11} = \left.\frac{\partial}{\partial i_d}\left(\frac{di_d}{dt}\right)\right|_{\mathbf{x}=\hat{\mathbf{x}}_{k|k-1}} = -\frac{R}{L_d}$$

$$F_{12} = \left.\frac{\partial}{\partial i_q}\left(\frac{di_d}{dt}\right)\right|_{\mathbf{x}=\hat{\mathbf{x}}_{k|k-1}} = \frac{L_q}{L_d}\hat{\omega}_{e,k|k-1}$$

$$F_{13} = \left.\frac{\partial}{\partial \omega_e}\left(\frac{di_d}{dt}\right)\right|_{\mathbf{x}=\hat{\mathbf{x}}_{k|k-1}} = \frac{L_q}{L_d}\hat{i}_{q,k|k-1}$$

$$F_{21} = \left.\frac{\partial}{\partial i_d}\left(\frac{di_q}{dt}\right)\right|_{\mathbf{x}=\hat{\mathbf{x}}_{k|k-1}} = -\frac{L_d}{L_q}\hat{\omega}_{e,k|k-1}$$

$$F_{22} = \left.\frac{\partial}{\partial i_q}\left(\frac{di_q}{dt}\right)\right|_{\mathbf{x}=\hat{\mathbf{x}}_{k|k-1}} = -\frac{R}{L_q}$$

$$F_{23} = \left.\frac{\partial}{\partial \omega_e}\left(\frac{di_q}{dt}\right)\right|_{\mathbf{x}=\hat{\mathbf{x}}_{k|k-1}} = -\frac{L_d\hat{i}_{d,k|k-1} + \lambda}{L_q}$$

$$F_{43} = \left.\frac{\partial}{\partial \omega_e}\left(\frac{d\theta_e}{dt}\right)\right|_{\mathbf{x}=\hat{\mathbf{x}}_{k|k-1}} = 1 \tag{26}$$

$$\mathbf{H}_{k-1} = \left.\frac{\partial h(\mathbf{x}(t))}{\partial \mathbf{x}}\right|_{\mathbf{x}=\hat{\mathbf{x}}_{k|k-1}} = \begin{bmatrix} 1 & 0 & 0 & 0 \\ 0 & 1 & 0 & 0 \end{bmatrix}$$

APPENDIX B

The following motor parameters are used for Simulink simulation:

TABLE II
DATA OF PMSM USED IN SIMULATIONS

Parameter	Symbol	Value
Stator winding self induction	L_s	32 mH
Stator winding resistance	R_s	5 Ω
Back EMF constant	K_e	0.215 V·s/rad
Damping	B	1.0 x 10^{-3} N·s/rad
Number of pole-pairs	P	2
Rotor inertia	J	0.6 x 10^{-3} kg·m^2
Nominal speed	ω_n	190 rad/s
Nominal Torque	T_n	2Nm
Drive current limit	I_{max}	16 A
Drive voltage limit	V_{max}	200V

REFERENCES

[1] S. Bolognani, M. Zigliotto and M. Zordan, "Extended-range PMSM sensorless speed drive based on stochastic filtering," *IEEE Trans. Power Electronics*, vol. 16, no. 1, Jan. 2001, pp. 110–117.

[2] S. Bolognani, L. Tubiana, M. Zigliotto, "EKF-based sensorless IPM synchronous motor drive for flux-weakening applications," *IEEE Trans. Industry Applications*, vol. 39, no. 3 , May-June 2003, pp. 768–775.

[3] R. Dhaouadi, N. Mohan and L. Norum, "Design and implementation of an extended Kalman filter for the state estimation of a permanent magnet synchronous motor," *IEEE Trans. Power Electronics*, vol. 6, no. 3 , July 1991, pp. 491–497.

[4] A. Bado, S. Bolognani and M. Zigliotto, "Effective estimation of speed and rotor position of a PM synchronous motor drive by a Kalman filtering technique," in *23rd Annual IEEE Power Electronics Specialists Conference, 1992. PESC '92 Record*, vol. 2, 29 June-3 July 1992, pp. 951–957.

[5] Young-Real Kim, Seung-Ki Sul, and Min-Ho Park, "Speed sensorless vector control of induction motor using extended Kalman filter," *IEEE Trans. Industry Applications*, vol. 30, no. 5 , Sept.-Oct. 1994, pp. 1225–1233.

[6] Che-Ming Lee and Chern-Lin Chen, "Speed sensorless vector control of induction motor using Kalman-filter-assisted adaptive observer," *IEEE Trans. Industrial Electronics*, vol. 45, no. 2, April 1998, pp. 359–361.

[7] S. Bolognani, R. Oboe and M. Zigliotto, "DSP-based extended Kalman filter estimation of speed and rotor position of a PM synchronous motor," in *20th International Conference on Industrial Electronics, Control and Instrumentation 1994, (IECON '94)*, vol. 3, 5-9 Sept. 1994, pp. 2097–2102.

[8] S. Bolognani, R. Oboe, and M. Zigliotto, "Sensorless full-digital PMSM drive with EKF estimation of speed and rotor position," *IEEE Trans. Industrial Electronics*, vol. 46, no. 1, Feb. 1999, pp. 184–191.

[9] K. L. Shi, T. F. Chan, Y. K. Wong and S. L. Ho, "Speed estimation of an induction motor drive using an optimized extended Kalman filter," *IEEE Trans. Industrial Electronics*, vol. 49, no. 1, Feb. 2002, pp. 124–133.

[10] M. Cernat, V. Comnac, R.-M Cernat and M. Cotorogea, "Sensorless control of interior permanent magnet synchronous machine using a Kalman filter," in *Proceedings of the 2000 IEEE International Symposium on Industrial Electronics, 2000 (ISIE 2000)*, vol. 2 , 4-8 Dec. 2000, pp. 401–406.

[11] S. Bolognani, L. Tubiana and M. Zigliotto, "Extended Kalman filter tuning in sensorless PMSM drives," *IEEE Trans. Industry Applications*, vol. 39 , no. 6 , Nov.-Dec. 2003, pp. 1741–1747.

[12] E.A. Wan and R. van der Merwe, "The Unscented Kalman filter for nonlinear estimation," in *Proceedings of the 2000 IEEE Symposium on Adaptive Systems for Signal Processing , Communication and Control (AS-SPCC)*, IEEE Press, 2000, pp. 153-158.

[13] S. J. Julier and J. K. Uhlmann, "A new extension of the Kalman filter to systems nonlinear systems," in *Proceedings of the 11th International Symposium on Aerospace/Defense Sensing, Simulation and Controls*, 1997.

[14] Simon Haykin, *Kalman Filtering and neural networks*. Communications Research Laboratory, McMaster University, Hamilton, Ontario, Canada, John Wiley & Sons, Inc. New York, ISBN 0-471-36998-5.

[15] S. J. Julier and H. F. Durrant-Whyte, "Navigation and parameter estimation of high speed road vehicles," in *Robotics and Automation, Conference*, pp. 101–105, 1995.

[16] R. van der Merwe and E. A. Wan, "Efficient derivative-free Kalman filters for online learning," in *European Symposium on Artificial Neural Networks (ESANN)*, Bruges, Belgium, 2001.

[17] B. Stenger, P. R. S. Mendonça and R. Cipolla, "Model-based hand tracking using an unscented Kalman filter," in *Proceedings of the British Machine Vision Conference*, September 2001, pp. 63-72.

[18] B. Akin, U. Orguner and A. Ersak, "State estimation of induction motor using unscented Kalman filter," in *Proceedings of 2003 IEEE Conference on Control Applications*, 2003 (CCA 2003), vol. 2, 23-25 June 2003, pp. 915–919.

[19] Paul Zarchan and Howard Mussoff, "Fundamentals of Kalman filtering: A practical approach," vol. 190, Progress in Astronautics and Aeronautics, American Institute of Aeronautics and Astronautics, Inc., ISBN 1-56347-455-7.

[20] A. R. Munoz and T. A. Lipo, "On-line dead-time compensation technique for open-loop PWM-VSI drives," *IEEE Trans. On Power Electronics*, vol. 14, no. 4, July 1999, pp. 683–689.

[21] Hyun-Soo Kim, Hyung-Tae Moon and Myung-Joong Youn, "On-line dead-time compensation method using disturbance observer," *IEEE Trans. On Power Electronics*, vol. 18, no. 6, Nov. 2003, pp. 1336–1345.

[22] Hyun-Soo Kim, Kyeong-Hwa Kim and Myung-Joong Youn, "On-line dead-time compensation method based on time delay control," *IEEE Trans. On Control Systems Technology*, vol. 11, no. 2, March 2003, pp. 279–285.

[23] Gene F. Franklin, J. David Powell and Michael Workman, *Digital Control of dynamic systems*. Addison Wesley Longman, Inc., 1998, ISBN 0-201-82054-44.

[24] Frank L. Lewis, *Applied Optimal Control & estimation: digital design & implementation*. Prentice-Hall, Inc., 1992, ISBN 0-13-040361-x.

NOMENCLATURE

TABLE III

Symbol	
L_s	Stator winding self induction
R_s	Stator winding resistance
K_e	Back EMF constant
B	Damping constant
P	Number of pole-pairs
J	Rotor inertia
ω_n	Nominal speed
v_A, v_B, v_C, i_A, i_B, i_C	Stator phase voltage and currents
v_d, v_d; i_d, i_q	Stator voltage and currents in rotor reference frame
v_α, v_β; i_α, i_β	Stator voltage and currents in stationary reference frame
v_γ, v_δ; i_γ, i_δ	Stator voltage in control coordinate reference frame
e_ω,e_β	Back EMF in stationary reference frame
p	Differential operator
ω_e	Angular velocity at electrical angle
ω_m	Angular velocity of mechanic rotor angle
T_e	Electrical torque
T_L	Load torque
L_d	Inductance of d axis
L_q	Inductance of q axis
T_s	Sample time
	Subscripts, superscripts, and symbols
a, b, c	Three axis frame quantities
d, q	Two axis synchronous frame quantities
α, β	Two axis stationary frame quantities
γ, δ	Two axis control frame quantities
‘	Transposed matrix
*	Reference quantities
^	Estimated
d	discrete